Applied Catalysis B: Environmental 165 (2015) 389–398

Contents lists available at ScienceDirect

Applied Catalysis B: Environmental

journal homepage: www.elsevier.com/locate/apcatb

Partial oxidation of methane over Ni^0/La_2O_3 bifunctional catalyst II: Global kinetics of methane total oxidation, dry reforming and partial oxidation

Tri Huu Nguyen [a,b,c,*], Agata Łamacz [a,**], Andrzej Krztoń [a], Agnieszka Ura [d], Karolina Chałupka [d], Magdalena Nowosielska [d], Jacek Rynkowski [d], Gérald Djéga-Mariadassou [e,1]

[a] Centre of Polymer and Carbon Materials Polish Academy of Sciences, M. Curie-Skłodowskiej 34, 41-819 Zabrze, Poland
[b] Silesian University of Technology, Faculty of Chemistry, M. Strzody 9, 44-100 Gliwice, Poland
[c] Saigon University, Faculty of Pedagogy of Natural Sciences, 273 An Duong Vuong Dis.5, HCMC, Viet Nam
[d] Lodz University of Technology, Institute of General and Ecological Chemistry, Zeromskiego 116, 90-924 Lodz, Poland
[e] University Pierre et Marie Curie, Paris, France

ARTICLE INFO

Article history:
Received 4 July 2014
Received in revised form 3 October 2014
Accepted 7 October 2014
Available online 16 October 2014

Keywords:
POM
Global kinetics
Power rate law
Nickel
La_2O_3

ABSTRACT

The global kinetics (power rate law) of methane total oxidation (TO) over La_2O_3 catalyst was performed at 773, 823 and 873 K. The global kinetics of methane dry reforming (DR) at 648, 673, 698 and 723 K and partial oxidation (POM) at 993, 1013, 1023 and 1053 K were conducted over Ni^0/La_2O_3 catalyst. The initial rate method and isolation method were used to determine initial rates, rate constants, and partial orders to reactants and establish the Arrhenius equations for TO, DR, POM. The experimental apparent activation energies were 87.8, 116.4 and 112.8 kJ mol^{-1} for DR, TO and POM, respectively. For TO, the reaction order to CH_4 was varying with conversion whereas that to O_2 was zero. For DR, the reaction order to CH_4 was constant, whereas that to CO_2 was dependent on the concentration of CO_2. The values of rate constants revealed the following order: $k_{DR} \gg k_{POM}$, k_{TO}. It was found that the rate constant of POM reaction is linked to that of methane TO: $k_{POM} \approx 2k_{TO}$. The catalytic cycle of methane TO is the "rate determining cycle" (rdc) of the POM process.

1. Introduction

This work is the second part of our study on the partial oxidation of methane (POM) carried out over Ni^0/La_2O_3.

Early work has shown that nickel was an active catalyst for the partial oxidation of methane (POM) to Syngas [1]. The earliest work was performed by Liander [2], Padovani and Franchetti [3] and Prettre et al. [4], who obtained high yields of syngas with 2:1 of H_2/CO molar ratio, within the temperature range from 1000 to 1200 K, at atmospheric pressure. Prettre et al. [4] were also among the first to report on the formation of synthesis gas by catalytic conversion of CH_4/O_2 mixtures in the experimental conditions of the present work, that is at a stoichiometric feed ratio with a methane to oxygen feed molar ratio of 2, over supported Ni at temperatures in the range of 973–1173 K. The reaction occurs in two stages. In the first stage methane is converted to CO_2 and H_2O until complete conversion of oxygen is achieved, since oxygen is the limiting reactant at a stoichiometric feed ratio. In the second stage syngas is produced via secondary reactions such as the carbon dioxide and steam-reforming reaction. According to Lundsford et al. [5,6] at a mechanistic level, over most catalysts partial oxidation involves total combustion of part of the CH_4, followed by reforming of the remaining CH_4 with CO_2 and H_2O.

Studies have already been published on the partial oxidation of methane over supported ruthenium catalysts [7,8] or using perovskite as precursor of catalysts [9]. According to Nishimoto et al. [10] partial oxidation of methane is also proceeding in two steps: total oxidation of methane to CO_2 and H_2O, followed by the methane reforming with CO_2 and H_2O.

Verykios and co-workers [11] investigated the reaction mechanism over the group of noble metals supported on Al_2O_3, SiO_2, and

* Corresponding author.
** Corresponding author.
E-mail addresses: huutri_sgu@yahoo.com (T.H. Nguyen), agata.lamacz@cmpw-pan.edu.pl (A. Łamacz).
[1] On leave.

http://dx.doi.org/10.1016/j.apcatb.2014.10.019
0926-3373/

TiO_2, and proposed the indirect production of syngas [12]. Recently, Forzatti and co-workers [13] developed a molecular kinetic scheme for methane partial oxidation over a Rh/α-Al_2O_3 catalyst according to an indirect reaction scheme also consisting of CH_4 deep oxidation with secondary reactions of CH_4 reforming responsible for syngas formation, the water–gas shift reaction, and consecutive oxidations of H_2 and CO.

Other mechanisms have been considered. Schmidt and co-workers [14,15] studied methane partial oxidation over Rh, Pt, and Rh/Pt and invoked a direct route to H_2 and CO. Baerns and co-workers [16–18] proposed a redox mechanism for metallic Rh and Rh/Al_2O_3 in which the initial step of methane dissociation is catalyzed by partially oxidized Rh sites, stabilized on the supported system. A direct reaction associated with a redox process of the metal has been proposed by Marin and co-authors [19,20]. The dissociation of methane and the formation of H_2 are occurring on reduced rhodium sites. The formation of CO proceeds via a redox cycle postulated by Mars and van Krevelen [21] selective oxidation reactions. The oxidation of the carbon adatoms to CO is accompanied by the reduction of rhodium oxide, which is reoxidized by incorporation of dioxygen into the catalyst. The authors reported that the product distribution is determined by the ratio of oxidized Rh (Rh_2O_3) to metallic Rh.

Recently, Tronconi and co-workers have presented a microkinetic approach of the mechanism of POM reaction. They used fundamental surface chemistry [22] in combination with detailed reactor modeling [23] for the microkinetic analysis of quasi-isothermal catalytic partial oxidation (CPO) experiments in an annular reactor [24–26]. This approach is similar to that used by Deutschmann and co-workers [27] for the steam and dry reforming of methane.

Concerning the mechanism of dry and steam-reforming, several proposals have been made. One of them is considering the CO_2 adsorption over the support oxide with the formation of surface carbonate species and a subsequent CO_2 dissociation. Zhang et al. [28] have shown that Ni/La_2O_3 catalyst provides a reaction pathway at the Ni–La_2O_3 interface. They suggested that CH_4 dehydrogenates on Ni crystallites, CO_2 being adsorbed on the La_2O_3 support or on the LaO_x species, which are decorating the Ni crystallites, in the form of $La_2O_2CO_3$ and formate species. According to Lercher and co-authors [29] the catalytic activity of zirconia supported platinum catalysts is determined by the accessibility of Pt on the Pt-ZrO_2 perimeter. This is linked to the CO_2 activation in the proximity of the Pt particles reacting with the methane activated on the metal. A strong metal-support interaction (SMSI) state on Pt/ZrO_2 during high temperature reduction has been considered but it does not persist under reaction conditions due to the presence of adsorbed oxygen from CO_2 dissociation. A bifunctional mechanism has been defined later by the same authors [30] CO_2 and CH_4 reacting via two different sites over Pt/ZrO_2. The main route to CO_2 reduction occurs via the initial formation of carbonate species close to the metal-support boundary. Carbon on the metal reduces that carbonate to formate by forming CO. Finally the formate decomposes rapidly to CO and a surface hydroxyl group. Hydroxyl groups recombine and form water or react further with methane to CO and hydrogen (steam reforming). Hydroxyl groups are participating in further mechanism developed by molecular kinetics and microkinetic approach. On Pt/TiO_2 Bradford and Vannice [31] found that active sites for reforming are also created in the Pt–TiO_x interfacial region. The influence of the support on catalyst activity appears to involve the adsorption and subsequent activation of CO_2 via the reverse water gas shift (RWGS). The support plays a role as a reservoir for surface hydroxyl groups, and the formation and subsequent decomposition of CH_xO species. A dual site mechanism was also proposed Schmal and co-authors [32,33] involving two different pathways over supported Rh on lanthanum-based solid: CH_4 decomposition on metal particles and CO_2 activation on the support. The reaction mechanism over Rh–lanthanum-based catalysts resembles that proposed by Tsipouriari and Verykios [34] for Ni/La_2O_3. These authors concluded that the formation of oxycarbonates during reaction plays a central role in the dry reforming of methane. CH_4 decomposes on the nickel crystallites to yield H_2 and adsorbed carbon that reacts with the oxycarbonate at the metal–support interface to liberate CO and at the same time clean up the metallic surface.

Resasco and co-authors [35] have taken into account that high conversions and a H_2/CO ratio near unity can only be achieved near 800 °C. They have concluded that the concepts developed from the studies conducted at lower temperatures can be not valid for the dry reforming reaction at high temperature. Furthermore, it has been shown [36] that hydroxyl groups remain on the surface of the zirconia up to 700 °C. But under industrially relevant conditions, these species may not play a role.

Rostrup-Nielsen and Bak Hansen [37] suggested that the mechanism of CO_2 reforming over metal-based catalysts does not differ significantly from that of steam reforming. The authors proposed that in both processes CH_4 total dehydrogenation is followed by the reaction with a surface O species, originated by either CO_2 or H_2O. Bradford and Vannice [38] extended this scheme and proposed for Ni-catalysts a generalized reaction scheme wherein surface hydroxyls originated by the reverse water gas shift react with CH_x species, emphasizing the analogy between CO_2 and steam reforming. Using Ni and noble metals, Wei and Iglesia [39] found a complete identity between the two processes. These authors also found [40] that the rate constants for H_2O (k_{H_2O}) and CO_2 (k_{CO_2}) reactions with CH_4 are identical within experimental accuracy at each reaction temperature. Activation energies were also similar for these two reactions.

Maestri et al. [25] have studied a microkinetic analysis of the steam and dry reforming of methane on Rh and developed an indirect scheme involving a primary reaction of CH_4 total oxidation to CO_2 and H_2O followed by the steam and CO_2 reforming of CH_4 producing syngas, and secondary reactions of water–gas shift and consecutive combustion of H_2 and CO. In the model methane suffers a dissociative chemisorption on Rh and dehydrogenates to C^*, where * is a rhodium active site, the overall elementary step being:

$$CH_4 + 5^* \rightarrow C^* + 4H^* \quad (1)$$

OH^*, provided by the dissociative adsorption of water into OH^* and H^*, oxidizes C^* to CO^*, according to:

$$C^* + OH^* \rightarrow CO^* + H^* \quad (2)$$

Similarly Deutschmann and co-workers [27] have detailed a multi-step reaction mechanism for modeling steam reforming of methane over nickel-based catalysts. The mechanism also includes partial and total oxidation reactions, water–gas shift reactions, formation of carbon monolayers, and methanation reactions. The reaction mechanism suggests that adsorbed carbon species CH_x(s) formed from activated methane react with adsorbed atomic oxygen O(s), formed from the adsorption of oxygen or from the decomposition of water and CO_2, and produce carbon oxide.

This microkinetic approach will be used in our future work for simulation of POM reaction over Ni^0/La_2O_3, according to our indirect model and is the basis for our indirect model approach.

In our previous paper [41], we have proposed an indirect model (Fig. 1) based on the coupling of three catalytic cycles (methane total oxidation (TO), dry reforming (DR) and steam reforming (SR)) for POM reaction over this bifunctional catalyst.

According to this mechanism the total oxidation of methane is occurring simultaneously with its dry reforming and steam reforming. It has been shown [41] that the TO of methane is occurring

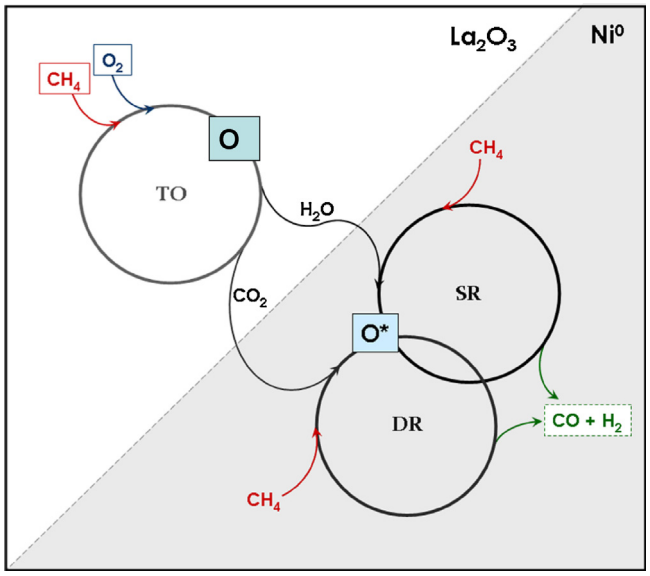

Fig. 1. POM model according to [41].

over the oxide active sites, i.e. La_2O_3. Neither DR nor SR is occurring over La_2O_3 but they take place over Ni^0. POM reaction is a high temperature catalytic process; for a stoichiometric mixture, at 1173 K, 100% conversion of reactants has been observed, the only detected products being CO and H_2 [41]. No CO_2 was observed and the ratio H_2/CO was near 2 that are consistent with the expected stoichiometric value of POM overall reaction [41]. It means that the CO_2 produced in TO reaction has been completely consumed by the DR reaction. It can be assumed that the DR reaction is occurring faster or at least with the same rate than that of TO. Moreover, many authors have reported that the rates of SR and DR are the same or that the SR rate is higher than that of DR [39,40,42].

In this paper, we shall compare the power rate laws at low conversion and the global rate constants of TO and DR and discuss what can be the rate determining cycle (rdc) of POM reaction. We shall detail the calculations of the initial rates, rate constants, partial orders to reactants and the apparent activation energies of TO and DR reactions (using the initial rate and isolation methods). Furthermore, for the first time, the initial rate, rate constant and apparent activation energy (E_a) of POM will be also determined. The initial rate method at low conversion and low contact times permits to calculate global rate constants in these particular conditions, similar to those of Bradford and Vannice [38], avoiding the problems of heat and mass transfers, remaining in kinetic control of the reaction and far thermodynamic equilibrium.

2. Experimental

2.1. Synthesis of Ni^0/La_2O_3 catalyst

According to our model, for sake of producing a good contact between La_2O_3 (production of CO_2 and H_2O) and Ni^0 (DR and SR consuming CO_2 and H_2O) and for optimizing the catalyst bifunctionality of the POM reaction, the lanthanum oxide supported nickel catalyst (Ni^0/La_2O_3) was synthesized using $LaNiO_3$ perovskite as precursor. The procedure of $LaNiO_3$ synthesis and its in situ transformation to Ni^0/La_2O_3 by flowing the stoichiometric POM reaction mixture ($CH_4/O_2 = 2$), have been described in details in our previous paper [41].

2.2. Catalytic tests

Catalytic rates study of methane TO, methane DR and POM were performed by placing samples (250–425 μm) in a quartz tube reactor (6 mm inner diameter) equipped with an external type-K thermocouple at the level of the catalyst bed, with continuous gas flow, at atmospheric pressure. Substrates, i.e. methane and oxygen or carbon dioxide were diluted in helium excepted for POM experiments where argon was used. The experiments were carried out at different temperatures, in isothermal conditions. Conversion degrees of methane less than 5–10% were used for determining the kinetic parameters.

The catalytic runs of methane TO were carried out on La_2O_3 (density of 1 g/cm^3); POM and DR reactions were studied over Ni^0/La_2O_3 (density of 0.6 g/cm^3), obtained by the transformation of $LaNiO_3$ in flowing POM mixture [41]. The weight of the catalyst samples were 0.1 g for all TO and DR experiments and less than 0.1 g for POM. The concentration of reagents at the reactor outlet was determined using an on-line gas chromatograph equipped with thermal conductivity detector (TCD).

Initial reaction rates, rate constants, partial orders to reactants and apparent activation energies of TO and DR experiments were determined by carrying out these reactions at different temperatures, reagents concentrations and total gas flow rates.

For the kinetic studies of POM reaction, the stoichiometric CH_4/O_2 ratio of 2 in the flowing gas mixture was applied for all experiments. The total gas flow rate was also identical for all runs. The variable reaction parameters were the reaction temperature and the weight of Ni^0/La_2O_3 sample.

3. Results and discussion

3.1. Global kinetic study of the total oxidation (TO) of methane on La_2O_3 catalyst

$$CH_4 + 2O_2 = CO_2 + 2H_2O \quad (3)$$

The kinetic study of methane TO was performed for methane conversion less than 10%. The values of initial rate (r^0), rate constant, partial orders to methane and oxygen, and activation energy of the overall reaction were determined using the initial rate and isolation methods.

In our previous work [41], methane TO over La_2O_3 has been carried out in the conditions of temperature programmed surface reaction (TPSR) permitting us to determine the temperature range (around 823 K) where conversions of methane and oxygen were ca. 5%. This domain of temperature was selected for the present experiments. The methane TO was carried out at three different temperatures: 773, 823 and 873 K, and for three different contact times (t_c): 0.06, 0.12 and 0.24 s. These low contact times and low methane conversions, similar to those used in the work of Bradford and Vannice [38] permitted to avoid the problems of heat and mass transfers. For each temperature the weight of catalyst sample was kept constant, maintaining constant the concentration of active sites, but the total gas flow rates were varying, i.e. 100, 50 and 25 ml min^{-1}. Five different ratios of CH_4/O_2 during TO catalytic tests were applied. The experimental conditions are presented in Table 1.

(i) In order to determine the partial order to methane (α), the apparent rate constant (k_{TO}) and the global E_a of reaction, the experiments denoted as Cases 1–3 were carried out with the initial methane concentration $[CH_4]_{init.}$ varying from 0.4 to 1.2 mol m^{-3}, while the initial oxygen concentration $[O_2]_{init.}$ was maintained constant at 0.8 mol m^{-3}.

Table 1
Experimental design of TO: for Cases 1–3:$[CH_4]_{init.}$ = 0.4–1.2 mol m^{-3}, while $[O_2]_{init.}$ remains constant at 0.8 mol m^{-3}. Cases 1, 4 and 5: $[O_2]_{init.}$ = 0.8–1.6 mol m^{-3}, whereas $[CH_4]_{init.}$ remains constant at 0.4 mol m^{-3}.

	$[CH_4]_{init.}/[O_2]_{init.}$	Total flow rate (ml min^{-1})	t_c (s)	T (K)
		100	0.06	
Case 1	0.4/0.8	50	0.12	
		25	0.24	
		100	0.06	
Case 2	0.8/0.8	50	0.12	
		25	0.24	773
		100	0.06	823
Case 3	1.2/0.8	50	0.12	873
		25	0.24	
		100	0.06	
Case 4	0.4/1.2	50	0.12	
		25	0.24	
		100	0.06	
Case 5	0.4/1.6	50	0.12	
		25	0.24	

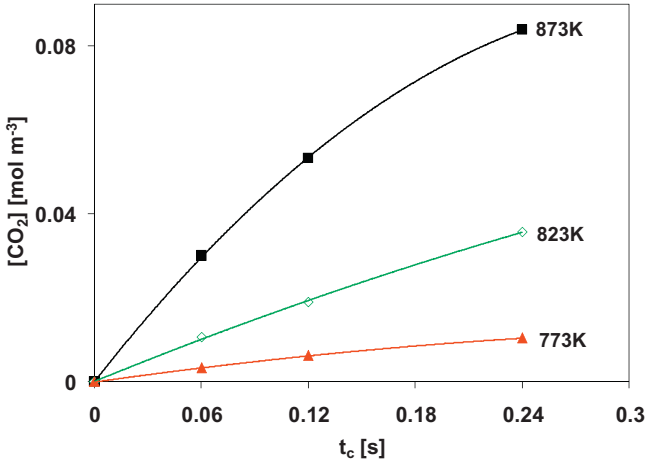

Fig. 2. CO_2 concentration vs. t_c during methane TO over La_2O_3 catalyst for Case 1: $[CH_4]_{init.}/[O_2]_{init}$ = 0.4/0.8 (Table 1).

(ii) For determining the partial order to oxygen (β), k_{TO} and E_a of the methane combustion in the Cases 1, 4 and 5, they were carried out with $[O_2]_{init.}$ varying from 0.8 to 1.6 mol m^{-3}, whereas $[CH_4]_{init.}$ was maintained constant at 0.4 mol m^{-3}.

(iii) As an example, Fig. 2 shows the kinetic graphs of CO_2 concentrations produced in TO (at three different temperatures) versus t_c for Case 1. It shows that the increases of concentration of CO_2 with t_c and with temperature are not linear.

The Eq. (4) was used to calculate the initial rates of reaction (r^0_{TO}) [mol m^{-3} s^{-1}]:

The overall reaction being:

$$CH_4 + 2O_2 = CO_2 + 2H_2O \quad (3)$$

$$r^0_{TO} = \frac{d[CO_2]}{dt} \quad (4)$$

r^0_{TO} being defined as the slopes of each graph for t_c = 0.

The r^0 values of methane TO (r^0_{TO}) for all Cases are presented in Table 2. For Cases 1–3 the values of r^0_{TO} are increasing with the increase of the concentration of methane introduced in the flowing gas mixture. It can be seen (Table 2) that the initial rate r^0_{TO} is not proportional to the increase of $[CH_4]_{init.}$ (at constant $[O_2]$). It means that the reaction order to methane is not constant. On the contrary, for Cases 1, 4 and 5 (at constant $[CH_4]_{init.}$), r^0_{TO} does not depend on the oxygen initial concentration (Table 2): one can conclude that the apparent reaction order to oxygen is zero.

The increase in temperature leads to the increase of r^0_{TO} for all cases.

Table 2
Initial rates of methane TO for all experiments. Cases 1–3: $[CH_4]_{init.}$ = 0.4–1.2 mol m^{-3}, while $[O_2]_{init.}$ is kept constant at 0.8 mol m^{-3}. Cases 1, 4 and 5: $[O_2]_{init.}$ = 0.8–1.6 mol m^{-3}, whereas $[CH_4]_{init.}$ is kept constant at 0.4 mol m^{-3}.

	$[CH_4]_{init.}/[O_2]_{init.}$	T (K)	r^0_{TO} (mol m^{-3} s^{-1})
		773	0.054
Case 1	0.4/0.8	823	0.178
		873	0.50
		773	0.06
Case 2	0.8/0.8	823	0.188
		873	0.58
		773	0.104
Case 3	1.2/0.8	823	0.25
		873	0.73
		773	0.051
Case 4	0.4/1.2	823	0.17
		873	0.50
		773	0.05
Case 5	0.4/1.6	823	0.178
		873	0.5

(iv) The values of α and k_{TO} for Cases 1, 2 and 3 (when $[O_2]_{init.}$ = const. = 0.8 mol m^{-3}) were calculated using the following Eqs. (5)–(8):

$$r^0_{TO} = k_{TO}[CH_4]^{\alpha}_{init.}[O_2]^{\beta}_{init.} \quad (5)$$

$$r^0_{TO} = k'_{TO}[CH_4]^{\alpha}_{init.} \quad \text{(for Cases 1–3)} \quad (6)$$

where

$$k'_{TO} = k_{TO}[O_2]^{\beta}_{init.} \quad (7)$$

$$\log r^0_{TO} = \log k'_{TO} + \alpha \log [CH_4]_{init.} \quad (8)$$

(v) The values of β and k_{TO} for Cases 1, 4 and 5, i.e. at constant concentration of methane ($[CH_4]_{init.}$ = 0.4 mol m^{-3}), were calculated using Eqs. (9)–(11).

$$r^0_{TO} = k''_{TO}[O_2]^{\beta}_{init.} \quad (9)$$

where

$$k''_{TO} = k_{TO}[CH_4]^{\alpha}_{init.} \quad (10)$$

$$\log r^0_{TO} = \log k''_{TO} + \beta \log [O_2]_{init.} \quad (11)$$

(vi) Fig. 3a presents the graph of $\log r^0$ vs. $\log [CH_4]_{init.}$, whereas $\log r^0$ vs. $\log [O_2]_{init.}$ is presented in Fig. 3b. The α and β values can be determined from the slope of the plots (respectively Fig. 3a and b). The values of $\log k'_{TO}$ and $\log k''_{TO}$ are calculated from the y-intercept of the plots at each temperature. It can be seen that α and $\log k'_{TO}$ are not constant. They are varying with the initial concentration of methane. In contrast, in Fig. 3b, the plots of $\log r^0$ vs. $\log [O_2]_{init.}$ are quasi-horizontal straight lines. Hence, the β value is equal to zero or near zero. The value of $\log k''_{TO}$ is constant too. The values of α, β and k'_{TO}, k''_{TO} are reported in Table 3.

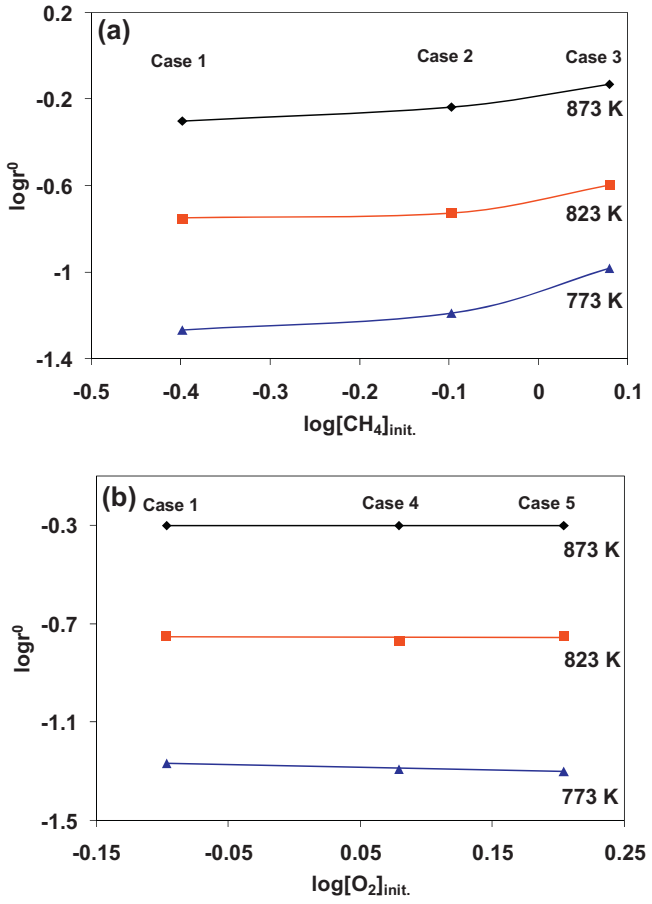

Fig. 3. Methane TO on La_2O_3: log r^0 vs. log $[CH_4]_{init.}$ (a) and log r^0 vs. log $[O_2]_{init.}$ (b) At three isotherms: 773–823–873 K.

Table 3
Values of α, k'_{TO} (mol m^{-3})$^{1-\alpha}$ s^{-1}, β, k''_{TO} (mol m^{-3})$^{1-\beta}$ s^{-1}.

T (K)	α	k'_{TO}	β	k''_{TO}
773	0.3 1.2	0.07 0.09	0	0.05
823	0.1 0.7	0.19 0.24	0	0.17
873	0.2 0.4	0.61 0.69	0	0.5

It can be seen that the value of the reaction order to oxygen (β) is zero. For sake of comparison with already published works on methane total oxidation we shall rather considered those using oxides as catalysts, the mechanism over supported precious metals [43–46] being different for both methane and dioxygen, as far the supported metal remains reduced. It has already been reported that the reaction order to oxygen was also zero or near zero during methane TO over single metal oxides, like La_2O_3 [47] or mixed metal oxides, such as $LaCr_{1-x}Ni_xO_3$ [48].

There was less agreement in the determined value of the reaction order to methane, as it depends on the experimental conditions (CH_4 or O_2 concentrations and temperature). Stojanovic et al. [48] calculated that the reaction order to methane varied from 0.5 to 1 over $LaCr_{1-x}NiO_3$ in the "573–773 K" temperature range. According to Toops et al. [47] the reaction order to methane in TO reaction over La_2O_3 at 848 and 948 K was 0.69 and 0.75, respectively. Under our experimental conditions (Table 3), the reaction order to methane was 0.3 and 1.2 at 773 K, 0.1 and 0.7 at 823 K and 0.2 and 0.4 at 873 K.

Table 4
Rate constants of methane TO (k_{TO}/(mol m^{-3})$^{1-\alpha}$ s^{-1}) at different temperatures.

T (K)	773	823	873
k_{TO}	0.08	0.22	0.65

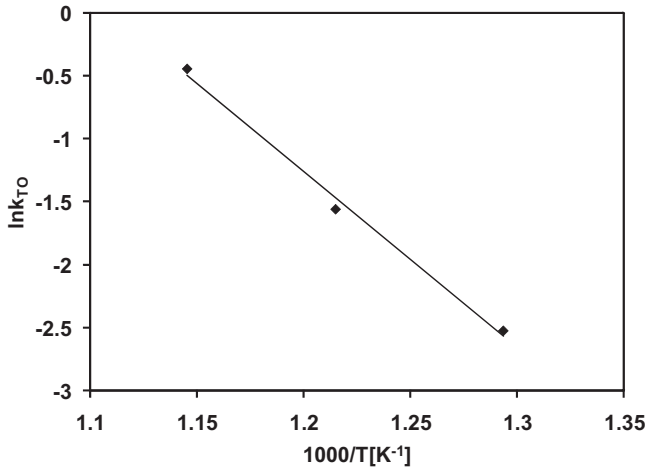

Fig. 4. Arrhenius plot of methane TO reaction over La_2O_3.

The values of the rate constant (k_{TO}) were calculated from Table 3, using Eqs. (7) and (10), both equations leading to the same value of k_{TO} as reported in Table 4.

The apparent activation energy of TO reaction (E_{aTO}) was determined with the Arrhenius equation (Eq. [12]), permitting for new experiments to calculate and compare the value of the rate constant at all temperatures (Fig. 4). The E_{aTO} over La_2O_3 was 116.4 kJ mol^{-1}. The resulting Arrhenius equation is:

$$\ln k_{TO} = 15.56 - \frac{116,422}{8.32 \times T} \quad (12)$$

The activation energy of methane TO reaction over alumina or silica supported Pd/Pt based catalyst is quite lower, about 86–92 kJ mol^{-1} [43–46]. In their experimental conditions (in the presence of an excess of H_2O), Giezen et al. [45] have reported that H_2O has some effect on the rate and activation energy of TO reaction. In this case the authors have found that the apparent activation energy was quite higher, being equal to 151 kJ mol^{-1}. In our work the E_{aTO} is 116.4 kJ mol^{-1} over La_2O_3, that is close to that reported by Toops et al. [47], i.e. 104.5 ± 8 kJ mol^{-1}. Furthermore Stojanovic et al. [48] have reported that the E_{aTO} over La_2O_3 was 139 kJ mol^{-1}.

3.2. *Kinetic study of methane DR on Ni^0/La_2O_3 catalyst*

The kinetic study of methane DR was determined in domains where methane conversion is less than 10%. The values of initial rates, rate constants, partial orders to methane and carbon dioxide, and the activation energy of the overall reaction (E_{aDR}) were determined using the initial rate and isolation methods.

According to Jozwiak et al. [49] the methane DR reaction was carried out over Ni^0/SiO_2 and the methane conversion was less than 10% at 623 K. Hence, we have chosen this temperature for our experiments conducted in the micro-reactor. The DR reaction was carried out at four different temperatures: 648, 673, 698 and 723 K, and three different contact times: 0.1, 0.2 and 0.4 s. For changing the contact time t_c, different total flow rates (100, 50, 25 ml min^{-1}) were applied, while the weight of the catalyst sample remained unchanged. We have considered five cases (Table 5), with different initial concentrations of reactants. In these conditions, methane and CO_2 conversions over Ni^0/La_2O_3 were about 5%.

Table 5
Experimental design of DR: For Cases 1–3:$[CH_4]_{init.}$ = 0.4 to 1.2 mol m^{-3}, while $[CO_2]_{init.}$ remains constant at 0.4 mol m^{-3}. Cases 1, 4 and 5: $[CO_2]_{init.}$ = 0.4 to 1.2 mol m^{-3}, whereas $[CH_4]_{init.}$ remains constant at 0.4 mol m^{-3}.

	$[CH_4]_{init.}/[CO_2]_{init.}$	Total flow rate (ml min^{-1})	t_c (s)	T (K)
		100	0.1	
Case 1	0.4/0.4	50	0.2	
		25	0.4	
		100	0.1	
Case 2	0.8/0.4	50	0.2	
		25	0.4	
		100	0.1	648
Case 3	1.2/0.4	50	0.2	673
		25	0.4	698
		100	0.1	723
Case 4	0.4/0.8	50	0.2	
		25	0.4	
		100	0.1	
Case 5	0.4/1.2	50	0.2	
		25	0.4	

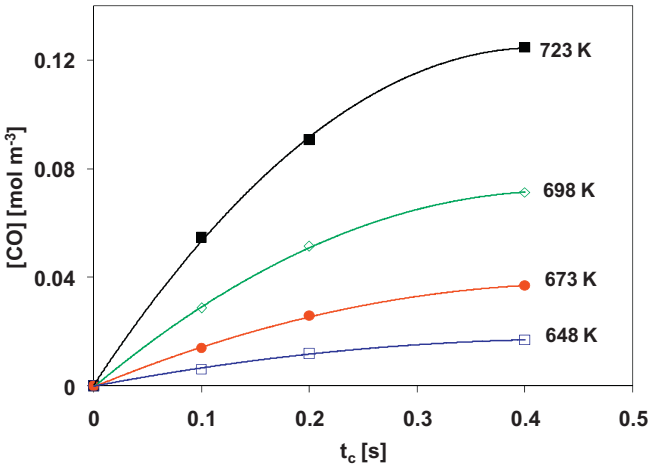

Fig. 5. CO concentration vs. t_c during methane DR over Ni^0/La_2O_3 catalyst for Case 1: $[CH_4]_{init.}/[CO_2]_{init}$ = 0.4/0.4 (Table 5).

(i) Experiments denoted as Cases 1–3 were conducted with $[CH_4]_{init.}$ varying from 0.4 to 1.2 mol m^{-3}. The initial CO_2 concentration ($[CO_2]_{init.}$) was always remaining at 0.4 mol m^{-3}. These experiments allowed us to determine the reaction order to methane (γ), the global rate constant (k_{DR}) and E_{aDR}.
(ii) During the experiments denoted as Cases 1, 4 and 5, the $[CO_2]_{init.}$ varied from 0.4 to 1.2 mol m^{-3}, while $[CH_4]_{init.}$ was always equal to 0.4 mol m^{-3}. These experiments led to the determination of the reaction order to CO_2 (δ), k_{DR} and E_{aDR}.
(iii) As an example, Fig. 5 shows the kinetic graph of CO concentration versus contact time for the Case 1 (i.e. CH_4/CO_2 ratio is 1). It can be observed that the CO production is not linear with contact time and temperature.
(iv) In order to calculate the initial rate (r^0_{DR}) of DR reaction (Eq. [13]), the Eq. [14] was used.

The overall reaction being:

$$CH_4 + CO_2 = 2CO + 2H_2 \quad (13)$$

$$r^0_{DR} = \frac{1}{2}\frac{d[CO]}{dt} \quad (14)$$

The values of r^0_{DR} for all Cases (with either only $[CH_4]_{init.}$ varying or only $[CO_2]_{init.}$ varying) are presented in Table 6. As expected, in each Case r^0_{DR} is increasing with temperature. Moreover, r^0_{DR} is also increasing with $[CH_4]_{init.}$.

Table 6
Initial rates (mol m^{-3} s$^{-1)}$ of methane DR for all experimental conditions. Cases 1, 2 and 3:$[CH_4]_{init.}$ = 0.4–1.2 mol m^{-3}, while $[CO_2]_{init.}$ is constant at 0.4 mol m^{-3}. Cases 1, 4 and 5: $[CO_2]_{init.}$ = 0.4–1.2 mol m^{-3}, whereas $[CH_4]_{init.}$ is constant at 0.4 mol m^{-3}.

	$[CH_4]_{init.}/[CO_2]_{init.}$	T (K)	r^0_{DR} = ½d[CO]/dt
		648	0.031
Case 1	0.4/0.4	673	0.07
		698	0.145
		723	0.275
		648	0.055
Case 2	0.8/0.4	673	0.12
		698	0.24
		723	0.425
		648	0.0695
Case 3	1.2/0.4	673	0.147
		698	0.288
		723	0.503
		648	0.048
Case 4	0.4/0.8	673	0.095
		698	0.183
		723	0.313
		648	0.035
Case 5	0.4/1.2	673	0.075
		698	0.15
		723	0.29

But in the case of the increase of $[CO_2]_{init.}$ (Cases 1, 4 and 5) the r^0_{DR} increases only for Cases 1–4, and decreases for Cases 4 to 5. This phenomenon will be explained below by considering the competitive adsorption between CH_4 and CO_2 over Ni^0, the active site where is occurring the dry reforming of methane with CO_2. Additionally, the $[CH_4]_{init.}$ has a higher impact on the increase of r^0_{DR} than $[CO_2]_{init.}$ This indicates that the reaction order to CO_2 can be lower than that for CH_4 in the global power rate law, as reported by Munera et al. over Rh/La_2O_3 [33].

(v) The reaction order to methane and CO_2 (γ and δ respectively) and the rate constant of methane DR (k_{DR}) can be determined from the values of r^0_{DR} presented in Table 6.
(vi) The values of γ and k_{DR} for Cases 1–3 (when $[CO_2]_{init.}$ = const. = 0.4 mol m^{-3}) were calculated using the following equations:

$$r^0_{DR} = k_{DR}[CH_4]^{\gamma}_{init.}[CO_2]^{\delta}_{init.} \quad (15)$$

$$r^0_{DR} = k'_{DR}[CH_4]^{\gamma}_{init.} \quad (\text{for Cases } 1-3) \quad (16)$$

where

$$k''_{DR} = k_{DR}[CO_2]^{\delta}_{init.} \quad (17)$$

$$\log r^0_{DR} = \gamma \log [CH_4]_{init.} + \log k'_{DR} \quad (18)$$

(vii) The values of δ and k_{DR} for Cases 1, 4 and 5, i.e. at constant concentration of methane ($[CH_4]_{init.}$ = 0.4 mol m^{-3}), were calculated using Eqs. (19)–(21).

$$r^0_{DR} = k''_{DR}[CO_2]^{\delta}_{init.} \quad (19)$$

where

$$k''_{DR} = k_{DR}[CH_4]^{\gamma}_{init.} \quad (20)$$

$$\log r^0_{DR} = \delta \log [CO_2]_{init.} + \log k''_{DR} \quad (21)$$

(viii) Fig. 6a shows the plots of log r^0 versus log $[CH_4]_{init.}$ (Eq. [18]). The dependence between log r^0 and log $[CO_2]_{init.}$ (from Eq. [21]) are presented in Fig. 6b. The γ and δ values were determined from the slopes of the graphs. The values of log k'_{DR} and

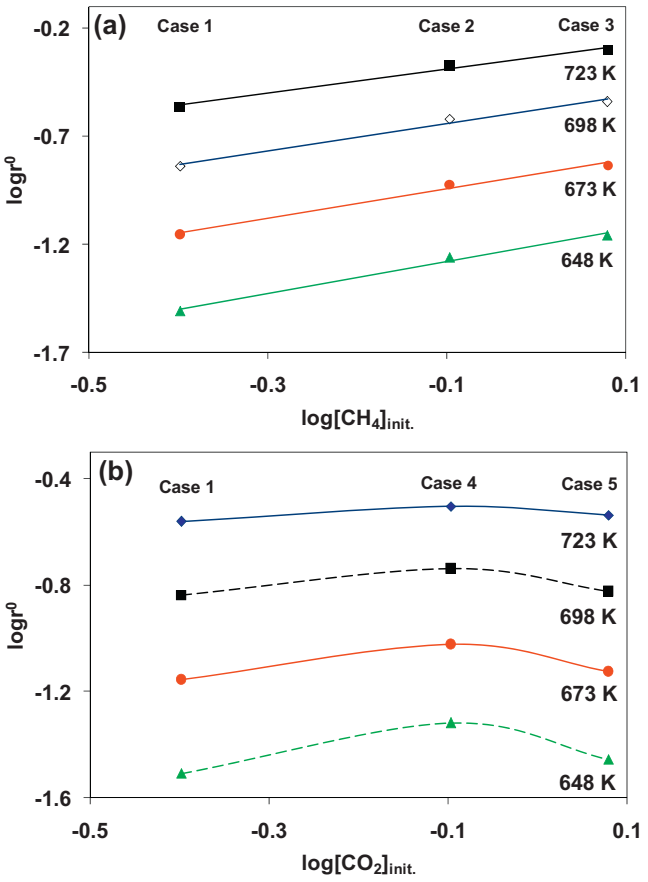

Fig. 6. Methane DR on Ni^0/La_2O_3: (a) log r^0 vs. log $[CH_4]_{init.}$ and (b) log r^0 vs. log $[CO_2]_{init.}$ at four isotherms 648, 673, 698 and 723 K.

log k''_{DR} are calculated from the *y*-intercept of the plots at each temperature.

It can be observed in Fig. 6a (Cases 1–3) that these plots are straight lines, hence the reaction order to CH_4 (γ) does not change with $[CH_4]_{init}$.

For Cases 1, 4 and 5 (Fig. 6b) the plots are not straight lines, so both the reaction order to CO_2 (δ) and log k''_{DR} depend on $[CO_2]_{init.}$ The change in the slope of the plots (Fig. 5b) from positive to negative for log $[CO_2]_{init.} > -0.1$ (i.e. when $[CO_2]_{init.} > 0.8$ mol m^{-3}, $[CH_4]$ being constant) is linked to the higher concentration and the stronger and competitive adsorption of CO_2 with CH_4 on the Ni^0 active sites of dry reforming, according to our model. Let's remember that the kinetic coupling of DR and SR cycles on Ni^0 for POM global system, made the competition of adsorption still stronger due to the additional simultaneous chemisorption of H_2O with CH_4 and CO_2. Let's note that when the temperature is high, at 723 K (Fig. 6b), the chemisorption of reactants on Ni^0 is decreasing and, consequently, the competition between CH_4, CO_2 and H_2O is decreasing and the slope of the chart is lower than at lower T (698, 673, 648 K).

The γ, δ, k'_{DR} and k''_{DR} values are shown in Table 7. It shows, differently than for Wei and Iglesia [39,40], that the order to methane is not 1 and the order to CO_2 different from zero. On the contrary our results are similar to those obtained by Bradford and Vannice [38], who reported that the reaction orders to methane and carbon dioxide are varying with the temperature and the nature of the oxide over which Ni^0 is supported (MgO, SiO_2, TiO_2). It is worth noting that our results are also similar to those of Munera et al. [33]. These authors have reported that the reaction orders to methane and carbon dioxide over Rh/La_2O_3 at 823 K were 0.61 and 0.37, respectively. Let's note that the sum of the two orders is near 1, in agreement with our classical kinetics to be published later.

Table 7
Reaction order to methane (γ) and CO_2 (δ), and rate constants (k'_{DR} (mol m^{-3})$^{1-\gamma}$ s^{-1}, k''_{DR} (mol m^{-3})$^{1-\delta}$ s^{-1}).

T (K)	γ	k'_{DR}	δ	k''_{DR}
648	0.74	0.062	0.63	0.055
			−0.78	0.040
673	0.69	0.134	0.44	0.105
			−0.58	0.084
698	0.64	0.264	0.34	0.197
			−0.49	0.164
723	0.56	0.466	0.19	0.327
			−0.19	0.301

Table 8
Rate constants of DR methane reaction (k_{DR} (mol m^{-3})$^{1-(\gamma+\delta)}$ s^{-1}) at different temperatures.

T (K)	648	673	698	723
k_{DR}	0.11	0.19	0.36	0.55

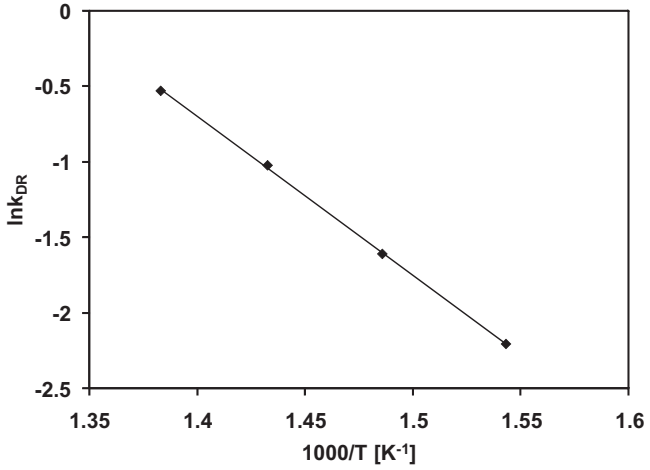

Fig. 7. Arrhenius plot of DR reaction over Ni^0/La_2O_3.

(ix) Finally the value of the rate constant of methane DR (k_{DR}) (Table 8) was calculated using Eqs. (17) and (20). The apparent activation energy of DR reaction (E_{aDR}) was determined using the Arrhenius equation (Eq. [22]), (Fig. 7). It will permit to calculate the value of the rate constant at higher temperatures where POM reaction is occurring.

The Arrhenius equation is:

$$\ln k_{DR} = 14.07 - \frac{87,776}{8.32 \times T} \quad (22)$$

The E_{aDR} is 87.8 kJ mol^{-1} for methane DR reaction carried out over Ni/La_2O_3. It is almost the same value as reported by other authors, for example 92, 96 and 109 kJ mol^{-1} for reaction carried out over Ni/MgO, Ni/SiO_2 and Ni/TiO_2, respectively [38], from 74 to 118 kJ mol^{-1} on Ni/Al_2O_3 [50–53] and 90 kJ mol^{-1} [54] or 107 kJ mol^{-1} [55] on modified Ni/Al_2O_3. Wei and Iglesia [39] reported that E_{aDR} over Ni/MgO was 105 kJ mol^{-1}, whereas Zhang and Verykios [56] reported, when the reaction was carried out on Ni^0/La_2O_3, that the E_{aDR} at the initial stage was 80 kJ mol^{-1} and 76 kJ mol^{-1} at the steady state, in very good agreement with our results.

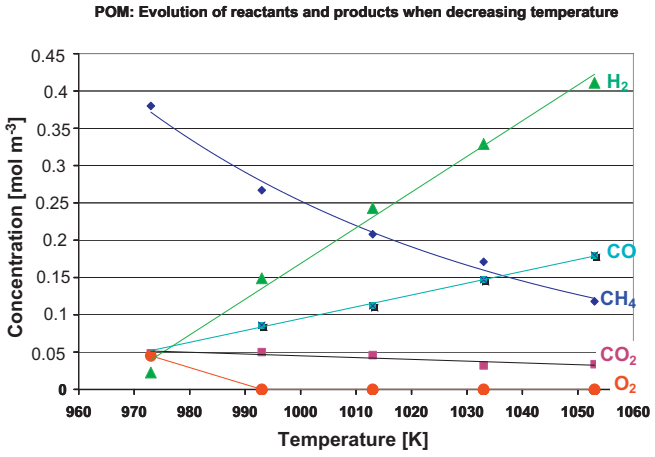

Fig. 8. Gas analysis evolution vs temperature of POM reactor.

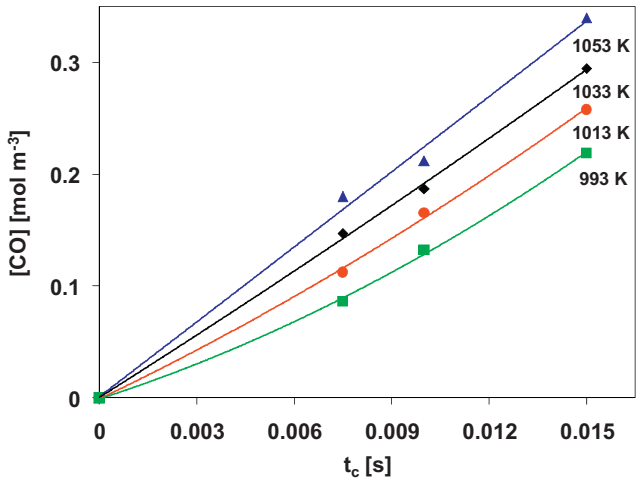

Fig. 9. CO concentration vs. t_c of POM reaction over Ni^0/La_2O_3 catalyst. $[CH_4]_{init} = 0.4\ mol\ m^{-3}$ and $[O_2]_{init.} = 0.2\ mol\ m^{-3}$.

3.3. Kinetic study of POM on Ni^0/La_2O_3 catalyst

The kinetic study of POM reaction (Eq. [24]) was performed at low conversion and contact time. The reaction feed being a stoichiometric POM gas mixture with $[CH_4]/[O_2] = 2$, a crucial question is related to the nickel oxidation state: is there any oxidation of the supported Ni^0 to NiO? The question is important as far only Ni^0 is active in steam and dry reforming in the global POM reaction and according to the indirect POM model (Fig. 1).

In order to control the absence of nickel oxidation, the kinetic experiment of POM reaction was conducted as follows: using the perovskite precursor, the final POM catalyst La_2O_3 supported Ni^0 was in situ prepared by flowing a stoichiometric POM feed up to 1173 K (900 °C). Then the kinetic data were obtained by decreasing the temperature from 1173 K to 993 K. As it can be seen in Fig. 8 the whole dioxygen of the feed was consumed by methane TO over La_2O_3 and there is no possible oxidation of Ni^0 to NiO in this 1053–993 K domain of temperature. As kinetics measurements have to be done at conversion less than 100%, CO_2 was detected as intermediate of the POM reaction, the WGS reaction at this high temperature being limited by the thermodynamic. The absence of NiO formation is consistent with the regular shape of CO and H_2 production occurring over Ni^0, and the values of the H_2/CO ratios remains near the stoichiometric value of 2. The Arrhenius plot (Fig. 10) of the POM reaction is the last proof for the absence of NiO in the TO reaction of the POM process. The molecular kinetics shows that:

$$k_{\exp} \text{ of POM} = k_{real\ of\ rds} \times [L] \quad (23)$$

$[L]$ being the density of Ni^0 sites exposed to the reaction. $[L]$ does not vary with the temperature (as far there is no sintering). Therefore, considering the Arrhenius law and the result for POM (Fig. 10), it comes: $\ln k_{real\ of\ rds} = \{A - \ln [L]\} - \{E_a/RT\}$ and the Arrhenius will not be linear if $[L]$ is varying with T, due to the oxidation of Ni to NiO.

The values of initial rate, rate constant, and activation energy of overall reaction were determined by the initial rate method. POM was performed in the micro reactor over Ni^0/La_2O_3 catalyst. It was carried out at four different temperatures 993, 1013, 1033 and 1053 K, using three different contact times 0.0075, 0.01 and 0.015 s; t_c was changed by changing the weight of the catalyst sample (15, 20 and 30 mg), while the total gas flow rate was 200 ml min^{-1}. The kinetic studies were performed with the stoichiometric O_2/CH_4 ratio (1/2). The $[CH_4]_{init.}$ was 0.4 mol m^{-3} and $[O_2]_{init.}$ was 0.2 mol m^{-3}. The kinetics of POM reaction over Ni^0/La_2O_3 was studied at the initial stage of syngas formation,

Table 9
Initial rate (mol m^{-3} s^{-1}) of POM reaction.

T (K)	993	1013	1033	1053
r^0_{POM}	10.34	14.45	18.67	22.50

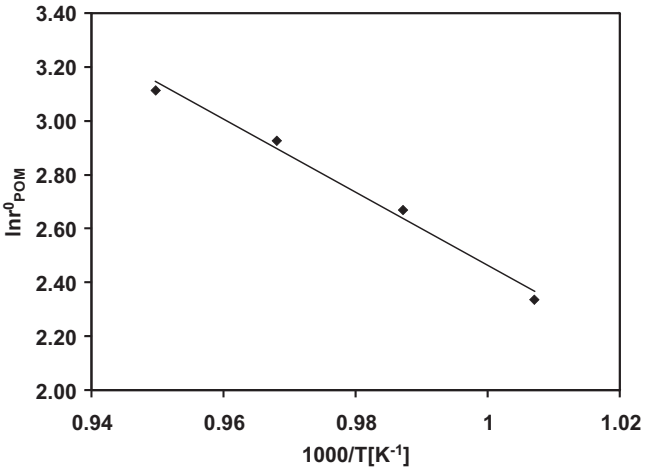

Fig. 10. Arrhenius plot of POM reaction over Ni/La_2O_3.

simultaneous with the total consumption of oxygen and when CO was produced in small amounts $\ll 0.04\ mol\ m^{-3}$.

Fig. 9 shows the kinetic graph of CO concentration versus t_c. It can be observed that the CO concentration plots are not linear with t_c for the four temperatures.

The overall POM reaction being:

$$CH_4 + 1/2O_2 = CO + 2H_2 \quad (24)$$

The initial rate was calculated using Eq. [22], at $t_c = 0$:

$$r^0_{POM} = \frac{d[CO]}{dt} \quad (25)$$

The values of r^0_{POM} at each temperature are presented in Table 9. The apparent activation energy of POM reaction (E_{aPOM}) was determined by the Arrhenius equation (Eq. [26]) corresponding to Fig. 10, where ln r^0 was used instead of ln k_{POM}, the initial concentrations of methane and oxygen being kept constant what can be the temperature. The E_{aPOM} over Ni^0/La_2O_3 catalyst was found to be 112.8 kJ mol^{-1}.

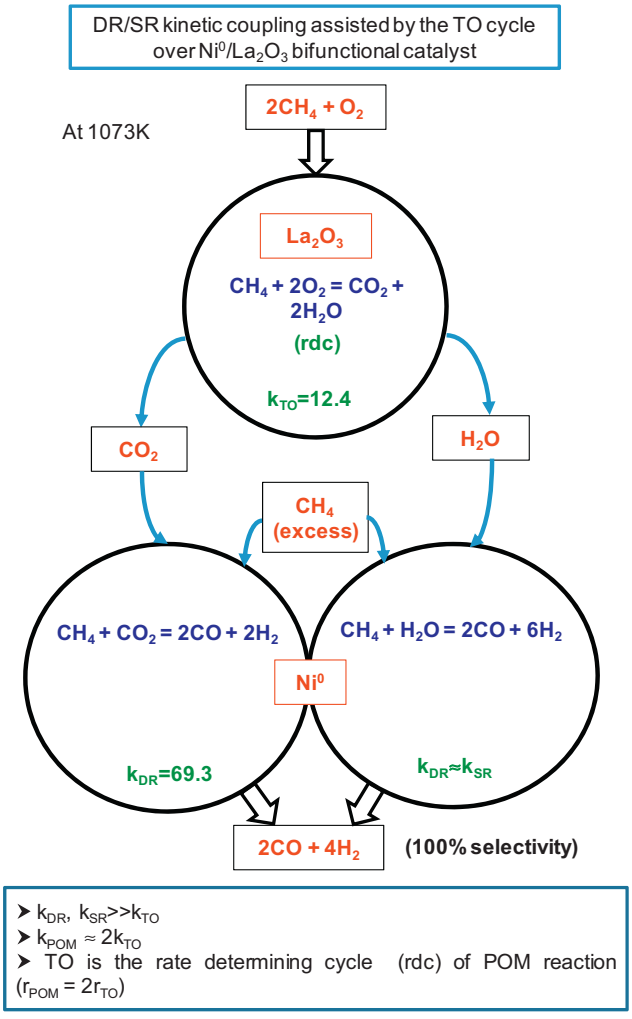

Fig. 11. Kinetically coupled DR and SR catalytic cycles over Ni^0 assisted by methane TO catalytic cycle. [41].

The Arrhenius law gives:

$$\ln k_{POM} = 16.02 - \frac{112,811}{8.32 \times T} \quad (26)$$

Since up to now, the E_{aPOM} has not been published in the literature, we cannot compare our result with others. But it is very interesting to compare the values of activation energies and rate constants of TO, DR and POM as determined in this work.

(i) It is very important to note that the values of E_{aTO} and E_{aPOM} are similar (116.4 and 112.8 kJ mol^{-1}, respectively), and both of them are higher than E_{aDR} (87.8 kJ mol^{-1}).
(ii) Moreover, the rate constant of DR is higher than the rate constants of TO and POM, which means that DR can occur much faster than POM and TO reactions.
(iii) In addition, the value of POM rate constant is about two times that of TO rate constant.

At 1073 K, $k_{DR} = 69.3$ $(mol\ m^{-3})^{1-(\alpha+\delta)}\ s^{-1}$, $k_{POM} = 29.47\ (mol\ m^{-3})^{1-\alpha}\ s^{-1}$ and $k_{TO} = 12.39\ (mol\ m^{-3})^{1-\alpha}\ s^{-1}$.

It is very important to explain why $k_{POM} \approx 2k_{TO}$ for justifying our model.

According to this model, POM reaction is the combination of three reactions: TO, DR and SR (Fig. 11) [41].

		σ	
TO:	$CH_4 + 2O_2 = CO_2 + 2H_2O$	1	(3)
DR:	$CH_4 + CO_2 = 2CO + 2H_2$	1	(13)
SR:	$CH_4 + H_2O = CO + 3H_2$	2	(27)
POM:	$4CH_4 + 2O_2 = 4CO + 8H_2$		(28)

(σ is the stoichiometric number: the number of times a reaction has to be used to get the overall POM reaction).

This sequence of global reactions can be represented as three catalytic cycles turning over simultaneously [41]: two of them (DR and SR) are kinetically coupled on Ni^0 active sites, assisted by the 3rd one (TO) delivering CO_2 and H_2O for DR and SR respectively.

Fig. 11 reports these cycles with all kinetics parameters determined in the present work.

The following questions are: (*a*) what is the rate determining cycle of POM global reaction and (b) why $k_{POM} \approx 2k_{TO}$?

Let's note that it has been found in literature that $k_{DR} \approx k_{SR}$ [39,40] that can be justified by the sequence of elementary steps [57] of DR and SR reactions, when considering that the rate determining steps, i.e. the dehydrogenation of methane in both DR and SR cycles, are the same; as a consequence, DR and SR reactions should have the same rate constant and subsequently the same rate of reaction as found by Wei and Iglesia [40].

Therefore, taking into account that:

$$E_{aTO} \approx E_{aPOM}$$

$$k_{DR} \approx k_{SR} \gg k_{POM} \approx 2k_{TO}$$

and

$$r_{DR} \approx r_{SR}$$

it can be concluded, as it will be shown below, that DR and SR cycles can turn over more rapidly than TO cycle, – the rates being also depending on reactant concentrations –, and the rate of POM can be strongly linked to the rate of TO of methane.

The factor 2 between k_{POM} and k_{TO} comes from the fact that for 1 turnover of TO cycle producing CO_2 and H_2O, the production of CO is 2 times the production of either CO_2 or H_2O (Eqs. [13] and (27)) from TO cycle. Fig. 11 clearly shows that for 1 CO_2 there are 2 CO, both DR and SR reactions producing CO; therefore, the rate constant of POM can be two times the rate constant of TO.

Hence, to verify if the methane TO cycle can be the rate determining cycle (rdc), i.e. the slowest one in POM process, the following initial rates can be separately calculated at 1073 K with $[CH_4]_{init.} = 0.4\ mol\ m^{-3}$ for all reactions:

- $r^0_{POM} = 29.5\ mol\ m^{-3}\ s^{-1}$
- $r^0_{TO} = 12.4[0.4]^{0.2} = 10.35\ mol\ m^{-3}\ s^{-1}$ (the order to O_2 is zero)

For r^0_{DR}, as there is no CO_2 in the POM feed, it can be calculated in the case where $[CO_2]_{initial} = 0.4\ mol\ m^{-3}$

- $r^0_{DR} = 69.3[0.4]^{\gamma}[0.4]^{\delta} = 27.7\ mol\ m^{-3}\ s^{-1}$

with $\gamma + \delta = 1$ (classical kinetics to be published later) and

- $r^0_{SR} = r^0_{DR} = 27.7\ mol\ m^{-3}\ s^{-1}$

It appears that $r^0_{TO} < r^0_{DR}, r^0_{SR}$ and

- $2r^0_{TO} = 20.7\ mol\ m^{-3}\ s^{-1}$ is near the value of r^0_{POM}.

The initial rate of production of syngas should be, in the presence of $[CO_2]_{initial} = 0.4\ mol\ m^{-3}$:

$r^0_{DR} + r^0_{SR} = 55.4\ mol\ m^{-3}\ s^{-1} \gg r^0_{POM}$.

It clearly appears that the *initial* rates of the DR and SR reforming cycles producing the syngas mixture cannot be that of POM due to

the instantaneous low concentrations of CO_2 and H_2O, but rather that of TO cycle during the POM process: in other words, according to the overall equation of POM (Eq. 28) (no CO_2, no H_2O), the DR and SR cycles are quickly (high rate constants) consuming CO_2 and H_2O with a rate regulated by the production of CO_2/H_2O delivered by the slower TO cycle.

It can be concluded that TO is the rate determining cycle of the overall POM process, that is the slower one.

4. Conclusion

According to the scheme of POM reaction over the bifunctional Ni^0/La_2O_3 catalyst (Fig. 11) [41], the total oxidation of methane (TO) occurs simultaneously with its dry (DR) and steam reforming (SR).

The global kinetics of POM was determined in the present work together with the kinetics of TO and DR, assuming with previous authors that the kinetics of SR is the same as for DR [39,40].

The kinetics of methane TO was studied over La_2O_3 alone, whereas the kinetics of DR and POM were studied over Ni^0/La_2O_3.

The global kinetic (power rate laws) study leads to the determination of the initial rate values, at very low conversion and low contact time, avoiding the problems of heat and mass transfers, as in the conditions of previous authors [38].

In the case of methane TO it was found out that the reaction order to CH_4 was not constant, and depending on the concentration of methane. The reaction order to oxygen was always zero. Hence, the kinetics of methane TO does not depend on O_2 concentration and E_{aTO} was found to be 116.4 kJ mol^{-1}.

For methane DR reaction, the reaction order to CH_4 was constant, whereas the order to CO_2 was dependent on the concentration of CO_2 and reaction temperature, with the corresponding E_{aDR} equal to 87.8 kJ mol^{-1}. The activation energy of POM was E_{aPOM} = 112.8 kJ mol^{-1} near that of E_{aTO}.

The rate constants of the reactions (k_{TO}, k_{DR}, k_{POM}) at 1073 K (current temperature for POM process) were estimated using the Arrhenius equations. The values of the rate constants revealed the following order: $k_{DR} \gg k_{POM} \approx 2k_{TO}$.

It was found out that the rate of POM reaction is near that of methane TO reaction. Consequently the catalytic cycle of methane TO is the "rate determining cycle" (rdc) of the POM process. The factor 2 between k_{POM} and k_{TO} comes from the kinetic coupling of DR and SR over Ni^0 active sites, assisted by the methane TO over La_2O_3. The Ni^0/La_2O_3 material is a bifunctional catalyst that can open future researches for still more active POM reaction catalysts, taking into account and applying the present conclusions: a higher POM rate needs for a still more active oxide catalyst for TO reaction.

The power rate laws (PRL) used in this paper were obtained in a domain of low methane conversion. As the reaction orders in the PRL are varying with the conversion, the next work on POM global reaction will deal with the classical kinetics approach, permitting to develop the kinetic simulation of the reaction to higher conversion, the global orders to reactants of the equivalent PRL being integrated in the classical kinetics rate equation.

Acknowledgements

Dr. M. Lewandowski is greatly acknowledged for providing lanthanum oxide material. The government of Vietnam is gratefully acknowledged for the grant (4915/QD-BGDDT) given to Tri Huu Nguyen to realize this work in Poland.

References

[1] Q. Zhu, X. Zhao, Y. Deng, J. Nat. Gas Chem. 13 (2004) 191.
[2] H. Liander, Trans. Faraday Soc. 25 (1929) 462.
[3] C. Padovani, P. Franchetti, Giorn. Chem. Ind. Appl. Catal. 15 (1933) 429.
[4] M. Prettre, Ch. Eichner, M. Perrin, Trans. Faraday Soc. 43 (1946) 335.
[5] J.H. Lunsford, Catal. Today 63 (2000) 165.
[6] D. Dissanayake, M.P. Rosynek, K.C.C. Kharas, J.H. Lunsford, J. Catal. 132 (1991) 117.
[7] M.G. Poirier, J. Trudel, D. Guay, Catal. Lett. 21 (1993) 99.
[8] J.B. Moffat, Y. Matsumura, Catal. Lett. 24 (1994) 59.
[9] A.T. Aschcroft, A.K. Cheethom, J.S. Foord, M.L.H. Green, C.P. Grey, A.J. Murrel, P.D.F. Vernon, Nature 344 (1990) 319.
[10] H.-A. Nishimoto, K. Nakagawa, N.-O. Ikenaga, T. Suzuki, Catal. Lett. 82 (2002) 161.
[11] Y. Boucouvalas, Z. Zhang, X.E. Verykios, Catal. Lett. 27 (1994) 131.
[12] T. Ioannides, X.E. Verykios, Catal. Lett. 47 (1997) 183.
[13] I. Tavazzi, A. Beretta, G. Groppi, P. Forzatti, J. Catal. 241 (2006) 1.
[14] D.A. Hickman, L.D. Schmidt, J. Catal. 138 (1992) 267.
[15] D.A. Hickman, E.A. Haupfear, L.D. Schmidt, Catal. Lett. 17 (1993) 223.
[16] O.V. Buyevskaya, D. Wolf, M. Baerns, Catal. Lett. 29 (1994) 249.
[17] O.V. Buyevskaya, D. Wolf, M. Baerns, Catal. Lett. 29 (1994) 261.
[18] O.V. Buyevskaya, K. Walter, D. Wolf, M. Baerns, Catal. Lett. 38 (1996) 81.
[19] E.P.J. Mallens, J.H.B.J. Hoebink, G.B. Marin, J. Catal. 167 (1997) 43.
[20] K.H. Hofstad, J.H.B.J. Hoebink, A. Holmen, G.B. Marin, Catal. Today 40 (1998) 157.
[21] P. Mars, D.W. van Krevelen, Chem. Eng. Sci. 3 (1954) 41.
[22] M. Maestri, D.G. Vlachos, A. Beretta, G. Groppi, E. Tronconi, AIChE J. 55 (2009) 993.
[23] M. Maestri, A. Beretta, T. Faravelli, G. Groppi, E. Tronconi, D.G. Vlachos, Chem. Eng. Sci. 63 (2008) 2657.
[24] M. Maestri, D.G. Vlachos, A. Beretta, P. Forzatti, G. Groppi, E. Tronconi, Top. Catal. 52 (2009) 1983.
[25] M. Maestri, D.G. Vlachos, A. Beretta, G. Groppi, E. Tronconi, J. Catal. 259 (2008) 211.
[26] A. Donazzi, M. Maestri, B.C. Michael, A. Beretta, P. Forzatti, G. Groppi, E. Tronconi, L.D. Schmidt, D.G. Vlachos, J. Catal. 275 (2010) 270.
[27] L. Maier, B. Schädel, K. Herrera Delgado, S. Tischer, O. Deutschmann, Top. Catal. 54 (2011) 845.
[28] Z. Zhang, X.E. Verykios, S.M. MacDonald, S. Affrossman, J. Phys. Chem. 100 (1996) 744.
[29] J.H. Bitter, K. Seshan, J.A. Lercher, J. Catal. 171 (1997) 279.
[30] J.H. Bitter, K. Seshan, J.A. Lercher, J. Catal. 176 (1998) 93.
[31] M.C.J. Bradford, M.A. Vannice, J. Catal. 173 (1998) 157.
[32] M.M.V.M. Souza, D.A.G. Aranda, M. Schmal, J. Catal. 204 (2001) 498.
[33] J.F. Múnera, S. Irusta, L.M. Cornaglia, E.A. Lombardo, D.V. Cesar, M. Schmal, J. Catal. 245 (2007) 25.
[34] V. Tsipouriari, X.E. Verykios, Catal. Today 64 (2001) 83.
[35] S.M. Stagg, E. Romeo, C. Padro, D.E. Resasco, J. Catal. 178 (1998) 137.
[36] K.S. Langner, K.J. Goldwasser, M. Houalla, D.M. Hercules, Catal. Lett. 32 (1995) 263.
[37] J.R. Rostrup-Nielsen, J.-H. Bak Hansen, J. Catal. 144 (1993) 38.
[38] M.C.J. Bradford, M.A. Vannice, Appl. Catal. A 142 (1996) 73.
[39] J. Wei, E. Iglesia, J. Catal. 224 (2004) 370.
[40] J. Wei, E. Iglesia, J. Catal. 225 (2004) 116.
[41] T.H. Nguyen, A. Łamacz, P. Beaunier, S. Czajkowska, M. Domański, A. Krztoń, T.V. Le, G. Djéga-Mariadassou, Appl. Catal. B 152–152 (2014) 360.
[42] A.K. Avetisov, J.R. Rostrup-Nielsen, V.L. Kuchaev, J.-H. Bak Hansen, A.G. Zyskin, E.N. Shapatina, J. Mol. Catal. A: Chem. 315 (2010) 155.
[43] L. Ma, D.L. Trimm, C. Jiang, Appl. Catal. A 138 (1996) 275.
[44] A.F.A. Silversand, C.U.I. Odenbrand, Appl. Catal. A 153 (1997) 157.
[45] J.C.V. Giezen, V.D. Bergg, J.L. Kleinen, A.J.V. Dillen, J.W. Geus, Catal. Today 47 (1999) 287.
[46] K. Muto, N. Katada, M. Niwa, Appl. Catal. A 134 (1996) 203.
[47] T.J. Toops, A.B. Walters, M.A. Vannice, Appl. Catal. A 233 (2002) 125.
[48] M. Stojanovic, C.A. Mims, H. Moudallal, Y.L. Yang, A.J. Jacobson, J. Catal. 166 (1997) 324.
[49] W.K. Jozwiak, M. Nowosielska, J. Rynkowski, Appl. Catal. A 280 (2005) 233.
[50] S. Wang, G. Lu, Energy Fuels 12 (1998) 248.
[51] L.M. Aparico, A.G. Ruiz, I.R. Ramoa, Appl. Catal. A 170 (1998) 177.
[52] O. Tokunaga, S. Ogasawara, React. Kinet. Catal. Lett. 39 (1989) 69.
[53] T. Horiuchi, K. Sakuma, T. Fukui, Y. Kubo, T. Osaki, T. Mori, Appl. Catal. A 144 (1996) 111.
[54] U. Olsbye, T. Wurzel, L. Mleczko, Ind. Eng. Chem. Res. 36 (1997) 5180.
[55] A.A. Lemonidou, L.A. Vasalos, Appl. Catal. A 228 (2002) 227.
[56] Z. Zhang, X.E. Verykios, Appl. Catal. A 138 (1996) 109.
[57] A. Donazzi, A. Beretta, G. Groppi, P. Forzatti, J. Catal. 255 (2008) 241.